Effect of Humidity on Thermal Performances of a Non-evacuated Parabolic Trough Solar Collector

N.Basbous*‡, M.Taqi*, N.Belouaggdia*

* Laboratoire d'Ingénierie et de Matériaux LIMAT, Equipe énergétique,

Faculté des sciences Ben M'sik, Université Hassan II-Mohammedia, Casablanca,

Morocco

(basbous.nabil@yahoo.fr, Moha_taqi@yahoo.fr, n.belouaggadia@gmail.com)

‡Corresponding Author; N.Basbous, Lotissement Dalia n°117 bouskoura casablanca, Tel: +212 662 267 870,

Received: 12.03.2015 Accepted:03.07.2015

Abstract- Parabolic trough collectors have become some of the important elements of solar power plants in recent years. These devices are usually located in dry deserts, however their widespread use leads us to expect such facilities of trough collectors in wetlands. In fact, the idea was to study a possible installation in Casablanca in the town of Morocco which is humid. As a result, heat transfers could be affected in the presence of water vapor when the annulus is air-filled at atmospheric pressure, thus it is interesting to design the PTC as a function of the effect of moisture. In this paper, a detailed numerical study is presented. First, the mathematical model is validated by the experimental results of Sandia laboratories in the USA. Then, an evaluation of the effect of humidity on thermos-physical properties of humid air is carried out to assess convective heat transfers. Later, we have calculated the optical properties of water vapor in order to take into consideration the participation of humid air in radiative heat transfers. Thereby, a numerical simulation has been performed in order to compare the performances of trough collectors between humid and dry areas.

Keywords Parabolic Trough Collector, Heat loss, Thermal efficiency, Humidity.

1. Introduction

Parabolic trough collectors emerged in the late 19^{th} and the beginning of 20^{th} century. The first patent was obtained in 1907, and the first well-known plant which used energy supplied by trough collectors was set-up in 1913 in Egypt. However, solar energy has not been a great success because of low oil prices. It was not until the 70^{s} when the price of oil soared. This paved the way to the development of the trough collectors. Presently, these devices are the most common among the thermal collectors, indeed PTCs provided over 90% of the capacity of concentrating solar power plant technology until the end of 2010 [1]. A PTC is constructed as a parabolic trough mirror that reflects solar radiation onto a heat collector element (HCE) placed in the focal line of the parabola. The whole system is supported by a steel structure equipped with a drive mechanism to follow the sun.

Several numerical and experimental studies have been carried out to evaluate the performances of a parabolic trough collector. Edenburn [2] studied the thermal performances of a parabolic trough collector using an analytical heat transfer model. The results are in good agreement with experimental data of Sandia laboratories in USA. Dudley et al. [3] developed a heat transfer model to predict thermal efficiency and heat losses of a PTC. The results are in reasonable agreement with measured data obtained by Sandia. Foristall [4] predicted the efficiency and heat losses of a PTC by using two heat transfer models based on one- and two- dimensional energy balances implemented in Engineering Equation Solver. He found that the two-dimensional energy balances is more suitable for long receivers. Garcia-Valladares [5] performed a

numerical simulation of single- and double- pass parabolic trough collector. The single-pass numerical model has been validated with experimental data of Sandia national laboratories. The double-pass configuration enhances thermal efficiency of the solar collector compared with the single pass. In recent years, models that are more sophisticated were performed based on a three dimensional heat transfer analysis taken into account the non-uniformity of the solar radiations that strike the absorber [6].

In this paper, a one dimensional heat transfer model is presented. The existing studies published previously about PTCs have never considered the effect of humidity on thermal performances of a PTC. The idea behind this work is to evaluate the thermal losses of a PTC installed in a wetland.

2. Model and Numerical Simulation

2.1. Mathematical model

The mathematical model adopted in this work is based on energy balances of the heat collector element and the reflector. It takes into account the direct solar normal irradiation incident on the mirror, optical losses, thermal losses, and heat gain into the heat transfer fluid (HTF) (Fig.1). For simplicity, we have made the following assumptions:

- Negligible conduction losses at the ends of the trough.
- Negligible absorptivity of the cover.

Average energy balances of each component of the HCE are written as follows:

For the cover,

$$m_c C_{pc} \frac{dT_c}{dt} = \phi_{r-c}^{cv} + \phi_{r-c}^{rad} - \phi_{c-amb}^{cv} - \phi_{c-amb}^{rad} \quad (1)$$

For the absorber tube (or the receiver),

$$m_r C_{pr} \frac{dT_r}{dt} = \phi_{ar} - \phi_{r-f}^{cv} - \phi_{r-c}^{cv} - \phi_{r-c}^{rad} \quad (2)$$

For the HTF,

- Enthalpy balance,

$$\frac{\partial}{\partial t}\int_{in}^{out} \rho h A dx = \dot{m}_{in}h_{in} - \dot{m}_{out}h_{out} + \frac{\partial}{\partial t}\int_{in}^{out} pA dx + \int_{in}^{out} V\frac{\partial p}{\partial x}Adx + \int_{in}^{out} \mu\left(\frac{\partial V}{\partial x}\right)^2 Adx + \phi_{r-f}^{cv} \quad (3)$$

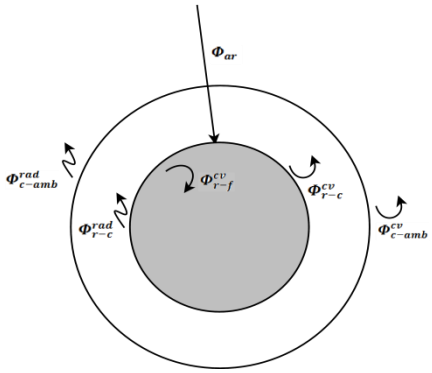

Fig. 1. Cross section of the heat collector element

- Mechanical energy balance,

$$A\frac{\partial}{\partial t}\int_{in}^{out} \rho\left(\frac{V^2}{2}+gz\right)dx = m_{in}\left(\frac{V^2}{2}+gz\right)_{in} - m_{out}\left(\frac{V^2}{2}+gz\right)_{out} - A\int_{in}^{out} V\frac{\partial p}{\partial x}Adx - A\int_{in}^{out}\mu\left(\frac{\partial V}{\partial x}\right)^2 Adx \quad (4)$$

h is the fluid mass enthalpy; p and V present the pressure and the speed of the fluid in a given section, respectively; x and $\dot{m}$ refer to the direction of the flow and the flow rate, respectively; T is the mean temperature; A and g are the receiver section and the gravity acceleration, respectively; and the subscripts $c, r, f,$ and amb stand for the cover, the receiver, the fluid and the ambience, respectively. The heat absorbed by the receiver ϕ_{ar} is [5]:

$$\phi_{ar} = \eta_0 C G_d A_{re} \quad (5)$$

η_0 is the optical efficiency defined as [7]:

$$\eta_0 = \rho_m \gamma_m \tau_c \alpha_r k_i F_m F_c F_{traking} \quad (6)$$

$\alpha_r, \tau_c, \rho_m, \gamma_m$ and k_i are, respectively, the receiver absorptance, cover transmittance, mirror reflectivity, shape factor, and the incident angle modifier. F_m and F_c take into account the fouling of the mirror, and the cover, respectively. $F_{traking}$ represents losses due to tracking errors. A_{re} and G_d are, respectively, the external receiver area and the direct solar radiation; C is the concentration ratio expressed by [8]:

$$C = \frac{W - D_{re}}{\pi D_{re}} \quad (7)$$

where W and D_{re} present the collector width and the external diameter of the receiver, respectively.

The heat exchanged by convection between the receiver and the HTF is expressed by the following correlation:

$$\phi_{r-f}^{cv} = h_{r-f} A_{ri}\left(T_r - T_f\right) \quad (8)$$

A_{ri} is the internal area of the receiver. h_{r-f} is the convection coefficient evaluated by the Dittus and Boetler correlations [10]:

$$\begin{cases} N_{u_f} = C_1 Re_f^{0.8} Pr_f^{0.4}, Re_f \geq 2300 \\ N_{u_f} = C_2 \qquad\qquad\quad , Re_f \leq 2300 \end{cases} \quad (9)$$

C_1 and C_2 are two coefficients which depend on the receiver geometry. N_{u_f} , Re_f and Pr_f are the Nusselt number, Reynolds number and Prandlt number of the fluid, respectively. The heat transfer by natural convection in a non-evacuated horizontal annulus under atmospheric pressure is estimated by the following correlations:

$$\phi_{r-c}^{cv} = h_{r-c}^{cv} A_{re}(T_r - T_c) \quad (10)$$

h_{r-c}^{cv} is the convection coefficient evaluated by [5]:

$$h_{r-c}^{cv} = \frac{2k_{eff}}{D_{re}\ln\left(\frac{D_{ci}}{D_{re}}\right)} \quad (11)$$

Where

$$\frac{k_{eff}}{k_{air}} = 0.317(Ra^*)^{\frac{1}{4}} \quad (12)$$

k_{air} and D_{ci} are, respectively, the thermal conductivity of the air and internal diameter of the cover. Ra^* is the modified Rayleigh number defined by [5]:

$$Ra^* = \left[\frac{ln\left(\frac{D_{ci}}{D_{re}}\right)}{(b')^{\frac{3}{4}}\left(\frac{1}{D_{re}^{\frac{3}{5}}}+\frac{1}{D_{ci}^{\frac{3}{5}}}\right)^{\frac{5}{4}}}\right]^4 Ra \quad (13)$$

where b' is the characteristic length defined by:

$$b' = \frac{D_{ci}-D_{re}}{2} \quad (14)$$

Ra is the Rayleigh number of the air:

$$Ra = \frac{g\beta_{air}b^3}{\nu_{air}\alpha_{air}}(T_r - T_c) \quad (15)$$

β_{air}, ν_{air} and α_{air} present the thermal expansion, the kinematic viscosity, and the thermal diffusivity of air in the annulus, respectively. In the case of vacuum in the annular space between the receiver and the annulus, h_{r-c}^{cv} is considered equal to zero.

The radiation heat transfer in the annulus without the participation of the air is estimated by the following equations [8]:

$$\phi_{r-c}^{rad} = h_{r-c}^{rad} A_{re}(T_r - T_c) \quad (16)$$

h_{r-c}^{rad} is the radiation heat transfer coefficient calculated by:

$$h_{r-c}^{rad} = \frac{\sigma\left(T_r^2+T_c^2\right)(T_r+T_c)}{\frac{1}{\varepsilon_r}+\frac{(1-\varepsilon_c)D_{re}}{\varepsilon_c D_{ci}}} \quad (17)$$

σ, ε_r and ε_c are, respectively, the Stefan-Boltzmann constant, the emissivities of the receiver and the cover.

The heat transfers between the cover and the ambience are described by:

$$\phi_{c-amb}^{cv} = h_{c-amb}^{cv} A_{ce}(T_c - T_{amb}) \quad (18)$$

$$\phi_{c-amb}^{rad} = h_{c-amb}^{rad} A_{ce}(T_c - T_{amb}) \quad (19)$$

A_{ce} is the external cover area.

In order to evaluate the convection coefficient h_{c-amb}^{cv}, we used Karlekar-Desmond and Churchill-Chu correlations [5]. The correlation of Karlekar-Desmond is expressed by as follows:

$$\begin{cases} h_{c-amb}^{cv}=0{,}989Re^{0{,}33}Pr^{1/3}\frac{k_{air}}{D_{ce}} & 0{,}4<Re\leq 40 \\ h_{c-amb}^{cv}=0{,}683Re^{0{,}486}Pr^{1/3}\frac{k_{air}}{D_{ce}} & 40<Re\leq 400 \\ h_{c-amb}^{cv}=0{,}193Re^{0{,}618}Pr^{1/3}\frac{k_{air}}{D_{ce}} & 400<Re\leq 4000 \\ h_{c-amb}^{cv}=0{,}0266Re^{0{,}805}Pr^{1/3}\frac{k_{air}}{D_{ce}} & 4000<Re\leq 40000 \end{cases} \quad (20)$$

The correlation of Churchill-Chu is expressed by:

$$h_{c-amb}^{cv} = \left(0.6 + 0.387\left(\frac{Ra}{\left(1+\left(\frac{0{,}559}{pr}\right)^{\frac{9}{16}}\right)^{\frac{16}{9}}}\right)^{\frac{1}{6}}\right)^2 \quad (21)$$

The value of the convection coefficient is taken as the maximum of these two correlations.

The exchange coefficient by radiation h_{c-amb}^{cv} between the cover and the ambience is evaluated by:

$$h_{c-amb}^{cv} = \varepsilon_c\sigma\frac{T_c^4-T_{sky}^4}{T_c-T_{amb}} \quad (22)$$

T_{sky} is the temperature of the sky considered as a black body [9] :

$$T_{sky} = 0{,}0552T_{amb}^{1.5} \quad (23)$$

2.2. Numerical simulation and validation of the model

In order to simulate heat losses and efficiency of the PTC in a steady state, we elaborated a program as illustrated in figure 2. The solution process involves iterations wherein the equations are solved sequentially until the solution converges. The validation of the simulation results is done with experimental data obtained in Sandia laboratories in the USA. We treated the case of an air-filled annulus at atmospheric pressure and we used in the simulation program the mean values of the operating conditions of experimental data (Direct normal insulation, wind speed and air temperature). The fouling of the mirror and the cover and the tracking errors are neglected in the validation program. The geometrical and optical characteristics of the LS-2 solar collector tested are shown in table 1. The HTF used was the Syltherm800. We approximated its thermos-physical properties such as density ρ_f , thermal conductivity λ_f, isobaric specific capacity C_{pf} , and dynamic viscosity μ_f by the polynomial regression method of data available on the website of the producer [12].

Those properties are temperature-dependent and are expressed as follows:

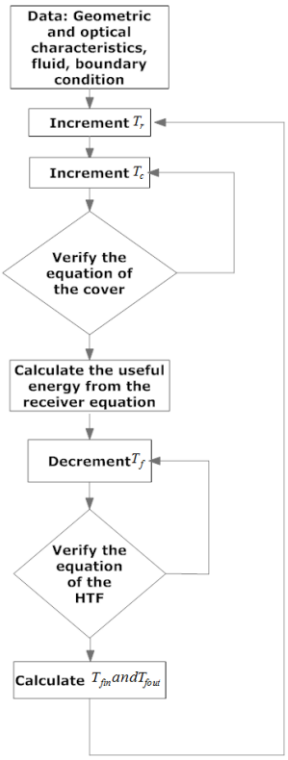

Fig. 2. Algorithm diagram

$$\rho_f = \sum_{i=0}^{4} r_i \left(T_f - 273.15\right)^i \quad (24)$$

$$C_{pf} = \sum_{i=0}^{4} c_i \left(T_f - 273.15\right)^i \quad (25)$$

$$\lambda_f = \sum_{i=0}^{4} l_i \left(T_f - 273.15\right)^i \quad (26)$$

$$\mu_f = \sum_{i=0}^{9} m_i \left(T_f - 273.15\right)^i \quad (27)$$

The polynomial coefficients of equations (24)-(27) are given in table 2. The figures 3a and 3b compare the numerical results and experimental data. Experimental measurements were made at approximately $50°C$ intervals up to $400°C$ to calculate efficiency and thermal losses. These calculations were based on mean data of values read from instruments (inlet and outlet temperatures of the HTF, flow rate, insolation...). Two error sources, statistical errors and instrument calibration errors, were combined using the root sum square method for the final error estimates of the PTC's performances, which are shown in the form of error bars in the figures 3a and 3b. Experimental values of useful energy q_u, efficiency η and heat loss q_{loss} were calculated by the following correlations:

$$q_u = \frac{\dot{m} C_{pf} (T_{fout} - T_{fin})}{C A_{re}} \quad (28)$$

$$\eta = \frac{q_u}{G_d} \quad (29)$$

$$q_{loss} = G_d(\eta_0 - \eta) \quad (30)$$

η_0 is the experimental value of optical efficiency. T_{fout} and T_{fin} are, respectively, the outlet and inlet temperatures. $\dot{m}$ is the flow rate of the fluid. Efficiency errors E_η are reported from results obtained by Dudley et al, they vary from 1.79% to 2.29%. The error estimates of heat loss $E_{q_{loss}}$ are considered as the same as those of heat gain E_{q_u}. They were calculated by the following correlation [11]:

$$E_\eta = \sqrt{\left(E_{q_u} \frac{\partial \eta}{\partial q_u}\right)^2 + \left(E_{G_d} \frac{\partial \eta}{\partial G_d}\right)^2} \quad (31)$$

$$E_{q_u} = E_{q_{loss}} = G_d \sqrt{E_\eta^2 - \left(E_{G_d} \frac{q_u}{G_d^2}\right)^2} \quad (32)$$

where E_G is the insolation error. Heat loss errors vary from $11.01\ W/m^2$ to $16.87\ W/m^2$.

Table 1. Optical and geometrical characteristics of the LS-2 tested [11]

Collector size $(L \times W)$	$7.8m \times 5m$
Absorber internal diameter	$0.066m$
Absorber external diameter	$0.07m$
Cover internal diameter	$0.109m$
Cover external diameter	$0.115m$
Rim Angle	$70\ degrees$
Focal length f	$1.84m$
Concentration ratio	71
Mirror reflectivity ρ_m	0.93
Shape factor γ_m	0.92
Cover transmittance τ_c	0.95
Absorber absorptance α_r	0.96
Absorber emittance ε_r	0.14
Incident angle modifier k_i	1

Table 2 Coefficients for the calculation of properties of Syltherm 800

$r_0 = 953.15371$ $r_1 = -0.91685$ $r_2 = 4.29364 \times 10^{-4}$ $r_3 = -1.70983 \times 10^{-6}$ $r_4 = 5.17311 \times 10^{-11}$	$c_0 = 1.57421$ $c_1 = 0.00171$ $c_2 = -3.37568 \times 10^{-8}$ $c_3 = 1.56318 \times 10^{-10}$ $c_4 = -2.15436 \times 10^{-13}$
$m_0 = 0.01506$ $m_1 = -3.56762 \times 10^{-4}$ $m_2 = 6.88393 \times 10^{-6}$ $m_3 = -1.0664 \times 10^{-7}$ $m_4 = 1.0892 \times 10^{-9}$	$m_5 = -6.8839 \times 10^{-12}$ $m_6 = 2.6559 \times 10^{-14}$ $m_7 = -6.0797 \times 10^{-17}$ $m_8 = 7.57675 \times 10^{-20}$ $m_9 = -3.95653 \times 10^{23}$
$l_0 = 0.13877$ $l_1 = -1.88145 \times 10^{-4}$ $l_2 = -1.03667 \times 10^{-10}$ $l_3 = 5.15575 \times 10^{-12}$ $l_4 = -1.22036 \times 10^{-14}$	

We could see that efficiency is within the margin of errors of experimental data (Fig.3b). As for thermal losses, a good degree of correlation has been obtained as they are within the margin of errors at low temperatures. However, for high temperatures, thermal losses are underestimated (Fig.3a). This can be justified by the increase in conduction losses that are neglected in the model. So the

mathematical model might be considered satisfactory for normal operating conditions of a PTC.

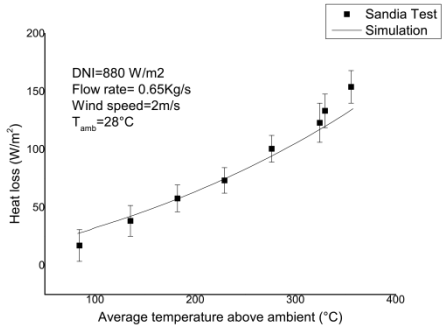

a.

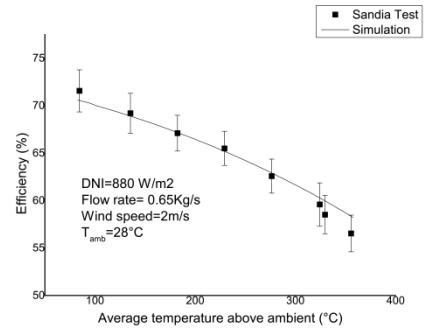

b.

Fig. 3. Comparison theory-experience. a. Thermal heat losses. b. Thermal efficiency

3. Effect of Humidity on a PTC

3.1. Effect of humidity on convective heat transfer

In order to assess the humidity effect on convective heat transfers in a parabolic trough collector, we assumed that the temperature of the ambient air does not exceed 40^0C, whereas the temperature of the air trapped in the annular space of the LS-2 collector evolves in the range of $[100°C, 260°C]$ in steady state at approximately the same operating conditions used in the validation. For the lack of available data of thermo-physical properties of moist air beyond $200°C$, we limited our study up to $200°C$. Therefore, we evaluated thermos-physical properties of moist air at ambient temperatures $(20°C, 30°C, 40°C)$ and at temperatures evolving between $100°C$ and $200°C$. To do this, humid air is regarded as a binary mixture of dry air and water vapor.

3.1.1. Density

The density of humid air is calculated according to the linear mixing equation for an ideal gas corrected by the compressibility factor to compensate for the real gas behavior [13]:

$$\rho_{ha} = \frac{1}{z_{ha}(x_v,T)} \frac{P_0}{RT} M_a \left(1 - x_v \left(1 - \frac{M_v}{M_a}\right)\right) \qquad (33)$$

Where $z_{ha}(x_v, T)$ and R are, respectively, the compressibility factor of the gas mixture and the universal gas constant. x_v is the molar fraction of water vapor. T is the temperature in Kelvin degree. M_v and M_a, are, respectively, the molar mass of water vapor and dry air. In the range of temperature $[0^0C, 100^0C]$ the compressibility factor is expressed as follows [13]:

$$z_{ha}(x_v, T) = z_{ha}(T) = 1 + AP_{sv} + BP_{sv}^2 \qquad (34)$$

$$P_{sv} = \sum_{i=0}^{4} C_i t^i \qquad (35)$$

$$A = D_1 + D_2 \, exp \frac{D_3}{T} \qquad (36)$$

$$B = E_1 + E_2 \, exp \frac{E_3}{T} \qquad (37)$$

where P_{sv} is the saturated vapor pressure in kPa, t is the temperature in Celsius degree. In the range of temperature $[100°C, 200°C]$, the compressibility factor is expressed as follows:

$$z_{ha}(x_v, T) = 1 + x_v \left(\frac{a+cT}{1+bT} - 1\right) \qquad (38)$$

The coefficients of the equations (34)-(38) are given in table A1. The figures 4a and 4b show the density of air as a function of the molar fraction of water vapor.

3.1.2. Viscosity

In this work, the viscosity of moist air $\mu_{ha}$is calculated in the range of temperature $[0°C, 100°C]$ on the basis of Wilke correlation of a mixture of dilute gases. Whereas in the range of $[100°C, 200°C]$, experimental data were fitted to find a function which could reproduce viscosity [14].

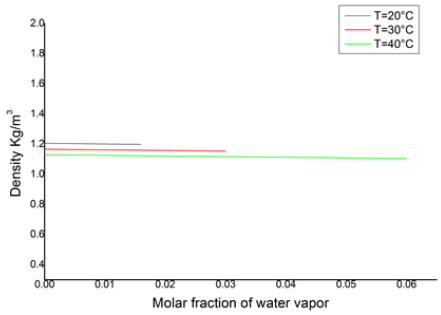

a.

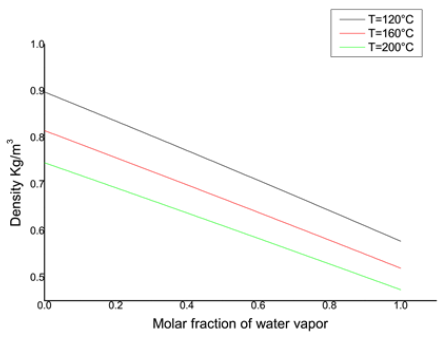

b.

Fig. 4. Density of humid air. a. Temperatures below $100°C$. b. Temperatures above $100°C$

$$\begin{cases} \mu_{ha} = \frac{(1-x_v)\mu_a}{(1-x_v)+x_v\phi_{av}} + \frac{x_v\mu_v}{x_v+(1-x_v)\phi_{va}} \\ for\ t \in [0°C, 100°C] \\ \mu_{ha} = [(H_0+H_1T)+(H_2+H_3T)x_v+(H_4+H_5T)x_v^2]10^{-6} \\ for\ t \in [100°C, 200°C] \end{cases} \quad (39)$$

where μ_a and μ_v are, respectively, the viscosity of dry air and water vapor in Ns/m^2 and are given by:

$$\begin{cases} \mu_a = (\sum_{i=0}^{4} F_i T^i)10^{-6} \\ \mu_v = (G_0 + G_1 t)10^{-7} \end{cases} \quad for\ t \in [0°C, 100°C] \quad (40)$$

The parameters ϕ_{av} and ϕ_{va} are defined as:

$$\begin{cases} \phi_{av} = \frac{\sqrt{2}}{4}\left(1+\frac{M_a}{M_v}\right)^{\frac{-1}{2}}\left[1+\left(\frac{\mu_a}{\mu_v}\right)^{\frac{1}{2}}\left(\frac{M_v}{M_a}\right)^{\frac{1}{4}}\right]^2 \\ \phi_{va} = \frac{\sqrt{2}}{4}\left(1+\frac{M_v}{M_a}\right)^{\frac{-1}{2}}\left[1+\left(\frac{\mu_v}{\mu_a}\right)^{\frac{1}{2}}\left(\frac{M_a}{M_v}\right)^{\frac{1}{4}}\right]^2 \end{cases} \quad (41)$$

The coefficients of the equations (40) are given in table A2. The figures 5a and 5b show the viscosity as a function of the molar fraction of water vapor.

3.1.3. Thermal conductivity

Thermal conductivity is calculated by the following correlations [13,14]:

$$k_{ha} = \frac{(1-x_v)k_a}{(1-x_v)+x_v\phi_{av}} + \frac{x_v k_v}{x_v+(1-x_v)\phi_{va}} \quad (42)$$

where ϕ_{av} and ϕ_{va} were defined in the previous section. k_a and k_v are given as follows:

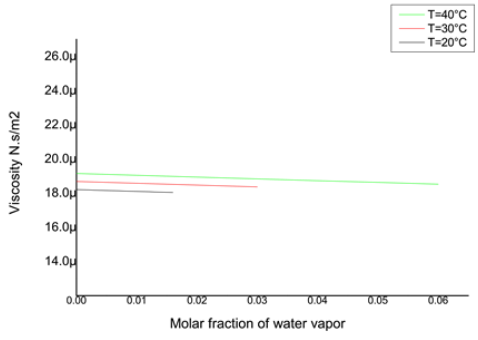

a.

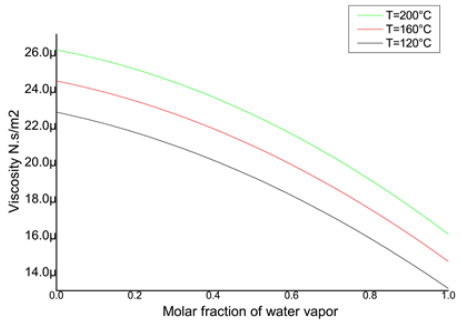

b.

Fig. 5. Viscosity of humid air. a. Temperatures below $100°C$. b. Temperatures above $100°C$

$$\begin{cases} k_a = \sum_{i=0}^{5} l_i T^i & for\ t \in [0°C, 100°C] \\ k_a = \sum_{i=0}^{3} M_i T^i & for\ t \in [100°C, 200°C] \end{cases} \quad (43)$$

$$\begin{cases} k_v = \sum_{i=0}^{2} J_i t^i & for\ t \in [0°C, 100°C] \\ k_v = \sum_{i=0}^{3} L_i T^i & for\ t \in [100°C, 200°C] \end{cases} \quad (44)$$

The coefficients of the equations (43) and (44) are given in table A3. The figures 6a and 6b show the thermal conductivity as a function of the molar fraction of water vapor.

3.1.4. Specific heat capacity

In the range of temperature $[0°C, 100°C]$, specific heat capacity is evaluated by a simple linear mixing equation and could be expressed as [13]:

$$c_{pha} = c_{pa}(1-x_v)\frac{M_a}{M_{ha}} + c_{pv}x_v\frac{M_v}{M_{ha}} \quad (45)$$

where M_{ha} is the molar mass of humid air which is expressed by:

$$M_{ha} = M_a(1-x_v) + M_v x_v \quad (46)$$

In the range of temperature [100°C,200°C], specific heat is obtained by a linear combination:

$$c_{pha} = c_{pa}(1-x_v) + c_{pv}x_v \quad (47)$$

The expressions of c_{pa} and c_{pv} are written as :

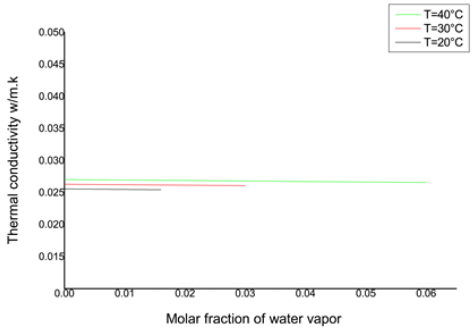

a.

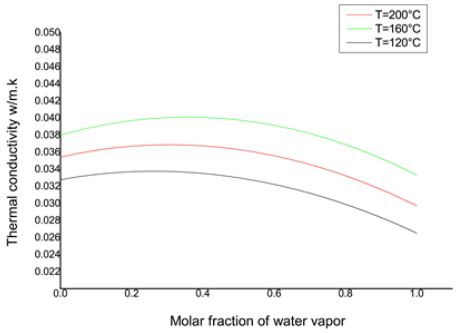

b.

Fig. 6. Thermal conductivity of humid air.
a. Temperatures below $100°C$. b. Temperatures above $100°C$

$$\begin{cases} c_{pa} = \sum_{i=0}^{4} K_i T^i & for\ t \in [0°C, 100°C] \\ c_{pa} = \sum_{i=5}^{8} K_i T^{i-5} & for\ t \in [100°C, 200°C] \end{cases} \quad (48)$$

$$\begin{cases} c_{pv} = \sum_{i=0}^{2} N_i t^i & for\ t \in [0°C, 100°C] \\ c_{pv} = \sum_{i=3}^{6} N_i T^{i-3} & for\ t \in [100°C, 200°C] \end{cases} \quad (49)$$

The coefficients of the equations (48) and (49) are given in table A4.

3.1.5. Thermal expansion

We based the evaluation of thermal expansion on its definition:

$$\beta_{ha} = \frac{1}{V_{ha}}\left(\frac{\partial V_{ha}}{\partial T}\right) = \frac{-1}{\rho_{ha}}\left(\frac{\partial \rho_{ha}}{\partial T}\right) \quad (50)$$

Values of thermal expansion are shown in Fig.8a and Fig.8b.

3.1.6. Result and discussion

We found that the effect of moisture on the properties of air is negligible for the usual temperatures of the atmosphere (Fig.4a, Fig.5a, Fig.6a, Fig.7a and Fig.8a). However, at high temperatures, these properties vary with humidity with the exception of the thermal expansion (Fig.4b, Fig.5b, Fig.6b and Fig.7b).

- Density and viscosity decrease when air becomes more humid.

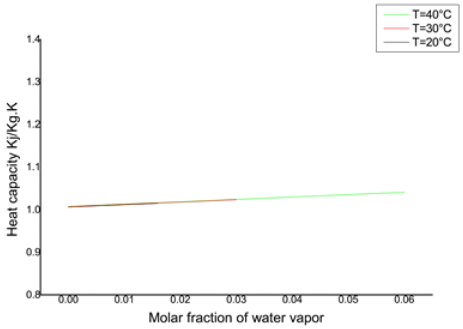

a.

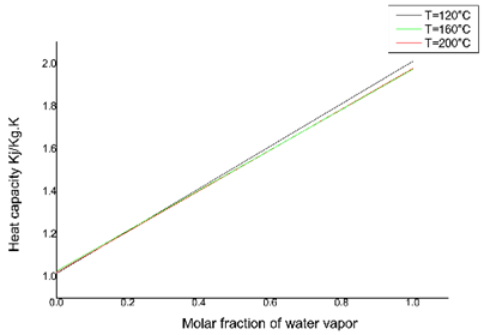

b.

Fig. 7. Specific heat capacity of humid air.
a. Temperatures below $100°C$. b. Temperatures above $100°C$

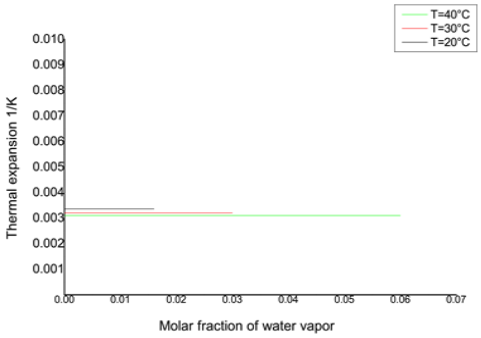

a

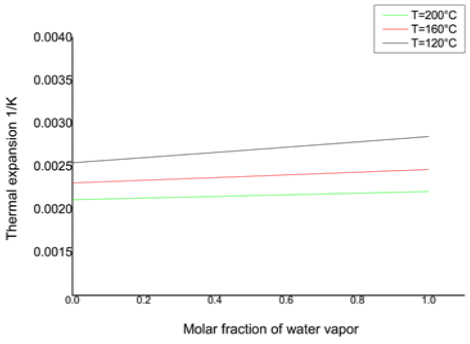

b

Fig. 8. Thermal expansion of humid air.
a. Temperatures below $100°C$. b. Temperatures above $100°C$

- The heat capacity increases linearly with moisture while the thermal conductivity varies just a little (Fig.7b and Fig.8b).

The study of the humidity effect on the convective heat transfers was carried out on a LS-2 collector. Humid ambient air isn't expected to affect the convective exchanges between the cover and the ambience, as its thermos-physical properties don't vary with humidity. The

annular space is assumed to be air-filled at atmospheric pressure. The convective heat transfer coefficient inside the annulus increases by about 6% when $x_v = 0.5$ and begins to decrease beyond this value. As for very high values of the molar fraction of the water vapor ($x_v > 0.9$), the convection coefficient becomes slightly smaller than that of dry air (Fig. 9). Consequently, the convective losses are expected to increase with humidity and get closer to those of dry air above 0.5, until becoming lightly smaller beyond 0.9. In fact, the increase in the convection losses may reach 8% for $x_v = 0.5$, whereas in the case of $x_v = 0.9$, the convection losses are very close to those of dry air (Fig. 10 and Fig. 11).

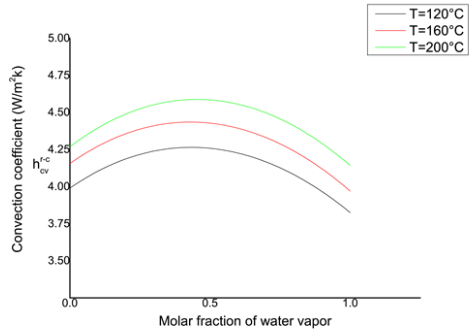

Fig. 9. The convection heat coefficient as a function of the molar fraction of water vapor.

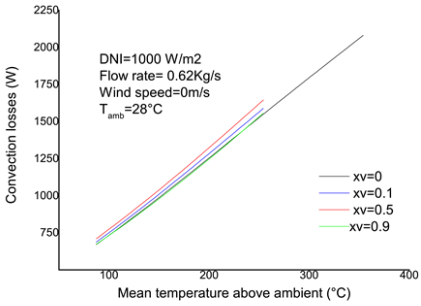

Fig. 10. Convection heat losses in the annulus as a function of temperature

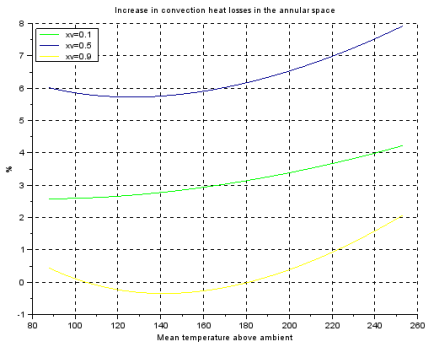

Fig. 11. Percentage increase in convection heat losses due to humidity vs mean temperature above ambient for different molar fraction of water vapor.

3.2. Effect of humidity on radiation heat transfers

3.2.1. Radiation model

This section will be devoted to the assessment of radiative losses in the annulus, taking into account the participation of water vapor affecting radiative transfers. According to the Net Radiation Method, the energy balance of radiative transfers in the annulus reads as follows:

$$\begin{cases} A_{re}J_r = A_{re}\varepsilon_r\sigma T_r^4 + \rho_r\left(\tau_g^{cr}F_{cr}A_{ci}J_c + A_{re}\varepsilon_{gr}\sigma T_g^4\right) \\ A_{ci}J_c = A_{ci}\varepsilon_c\sigma T_c^4 + \rho_c\begin{pmatrix}\tau_g^{cr}F_{rc}A_{re}J_r + \tau_g^{cc}F_{cc}A_{ci}J_c + \\ A_{ci}\varepsilon_{gc}\sigma T_g^4\end{pmatrix} \end{cases} \quad (51)$$

where ρ_i is the reflectivity of the element i. $F_{ij}$and τ_g^{ij}present the shape factor and the transmissivity of the gas mixture in ij direction, respectively. The subscript g refers to the gas mixture (humid air). The thermal radiative losses in the annular space are calculated from the following equation:

$$\phi_{r-c}^{rad} = A_{re}J_r - \tau_g^{cr}F_{cr}A_{ci}J_c - A_{re}\varepsilon_{gr}\sigma T_g^4 \quad (52)$$

3.2.2. Optical properties of humid air

The humid air is mainly a mixture of gases O_2, N_2, H_2, CO_2, and H_2O in different proportions. However, at high temperatures, the participation of gases with symmetrical molecules such as O_2 in radiative exchanges is negligible due to the absence of an absorption spectrum at these temperatures. As a result, only CO_2 and H_2O gases affect the thermal radiation. We limited our study to the effect of water vapor because moist air can contain significant amounts of water vapor especially at high temperatures, whereas the fraction of carbon dioxide is negligible. The radiative properties of the water vapor depend on the following parameters [15]:

- Mean beam length (MBL): it was introduced for the first time by Hottel to assess the effect of geometry on the radiative exchange between an isothermal gas and its boundaries and could be expressed as follows [16]:

$$L_e = \frac{4V}{A} \quad (53)$$

where V and A are, respectively, the volume and boundary of the medium (annular space).

- The radiation temperature of the gas, evaluated by:

$$T_g^2 = \frac{D_{ci}^2 T_c^2 + D_{re}^2 T_r^2}{D_{ci}^2 + D_{re}^2} \quad (54)$$

- Partial pressure of the water vapor P_v and total pressure of the gas mixture P_0 (or humid air).
- The temperature of the emitting source affects the absorption coefficient of the gas.

The following equations are used for calculating the total emissivity of humid air [15]:

$$\varepsilon_g\,(T_g;\, P_v L_e) = C_{H_2O}\,\varepsilon_g^0 \quad (55)$$

where ε_g^0 is the initial formula that calculate the emissivity, and C_{H_2O} is the correction factor. Their expressions are as follows:

$$log\left(\varepsilon_g^0\right) = \frac{a + \sum_{i=0}^{3}\left[b_i T^i + d_i\,(log\,(P_v L_e))^i\right]}{1 + \sum_{i=4}^{6}\left[b_i T^{i-3} + d_i\,(log\,(P_v L_e))^{i-3}\right]} \quad (56)$$

$$C_{H_2O} = \frac{a + \sum_{i=1}^{3}\left[b_i'\left(\frac{P_v+P_0}{2}\right)^i + d_i'(log\,(P_v L_e))^i\right]}{1 + \sum_{i=4}^{6}\left[b_i'\left(\frac{P_v+P_0}{2}\right)^{i-3} + d_i'(log\,(P_v L_e))^{i-3}\right]}. \quad (57)$$

The constants to be used in the equations (56) and (57) are summarized in table A5.

The absorptivity of humid air is evaluated as follows:

$$\alpha_g = \left(\frac{T_g}{T_s}\right)^{0.45} \varepsilon_g\left(T_s, P_v L_e\left(\frac{T_s}{T_g}\right)\right) \quad (58)$$

where T_s is the temperature of the emitting source.

The transmissivity of moist air is expressed by:

$$\tau_g \cong 1 - \alpha_g \quad (59)$$

The radiative properties of the air in the annulus are expressed from the above equations, by:

$$\varepsilon_{gr} = \varepsilon_{gc} = \varepsilon\,(T_g, P_v L_e) \quad (60)$$

$$\begin{cases} \alpha_g^{rc} = \left(\frac{T_g}{T_r}\right)^{0.45} \varepsilon\left(T_r, P_v L_e^{rc}\left(\frac{T_r}{T_g}\right)\right) \\ \alpha_g^{cr} = \left(\frac{T_g}{T_c}\right)^{0.45} \varepsilon\left(T_c, P_v L_e^{cr}\left(\frac{T_c}{T_g}\right)\right) \\ \alpha_g^{cc} = \left(\frac{T_g}{T_c}\right)^{0.45} \varepsilon\left(T_c, P_v L_e^{cc}\left(\frac{T_c}{T_g}\right)\right) \end{cases} \quad (61)$$

L_e^{ij} is the mean beam length in ij direction, τ_g^{ij} is approximated by:

$$\tau_g^{ij} = 1 - \alpha_g^{ij} \quad (62)$$

Optical properties of moist air are shown in Fig.12, Fig.13a, Fig.13b and Fig.13c. We found that the emissivity of the air increases with the amount of water vapor and decreases slightly with temperature (Figure 14). However, the transmissivity decreases with moisture and increases with the temperatures of the gas and the emitting source (Fig.13a, Fig.13b and Fig.13c).

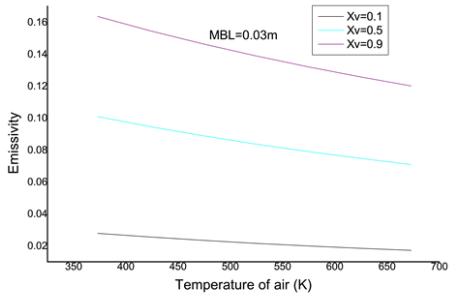

Fig. 12. Emissivity of moist air as a function of the temperature and the molar fraction of water.

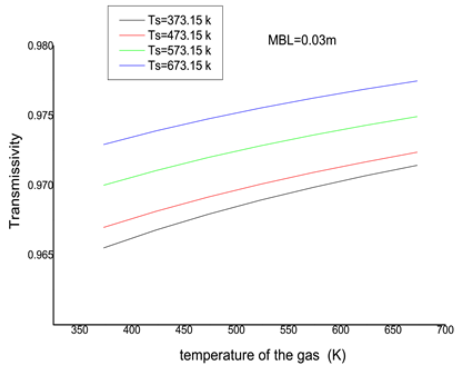

a

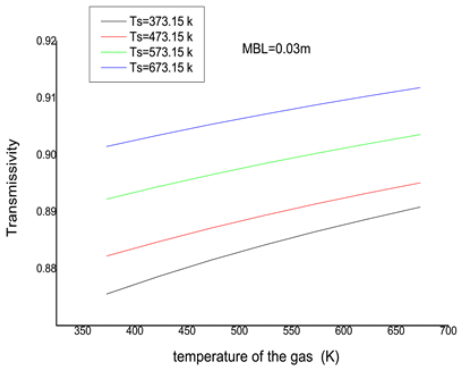

b

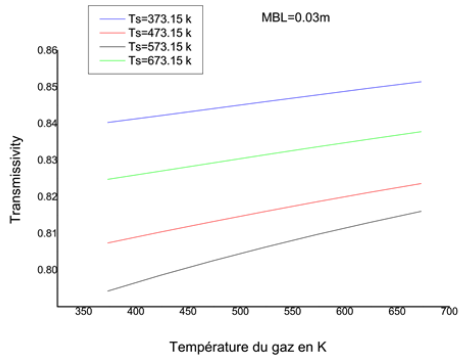

c

Fig. 13. Transmissivity of humid air as a function of temperature. a. In the case of the molar fraction $x_v = 0.1$. b. In the case of the molar fraction x_v=0.5. c. In the case of the molar fraction $x_v = 0.9$

3.2.3. Results and discussion

In this work, a simulation of thermal performances of a parabolic trough collector has been performed taking into account the humidity of the air trapped in the annulus. Both radiative and convective transfers are calculated based on optical and transport properties of moist air. The results show that radiative losses decrease with humidity (Fig. 14). The decrease of the percentage is between 3.5% and 7% (Fig. 15). Overall loss coefficient rises for low values of the molar fraction of the water vapor ($x_v \leq 0.5$), whereas it drops in very wet environments ($x_v = 0.9$). This is quite expected as convective heat losses increase for low humidity. However, total heat losses and thermal efficiency are slightly affected due to low values of the emissivity of the moist air present in the annulus and the negligible absorptivity of the visible radiations of water vapor.

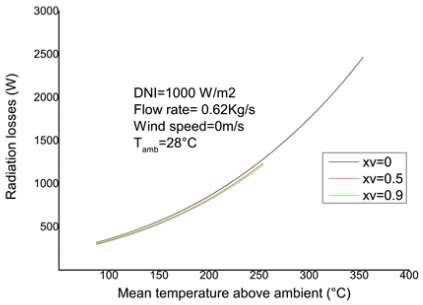

Fig. 14. Radiation heat losses in the annulus as a function of the amount of water vapor.

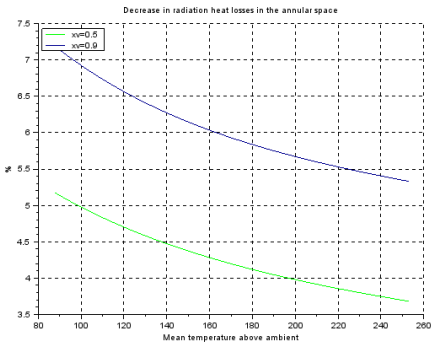

Fig. 15. Percentage decrease in radiation heat losses in the annular space

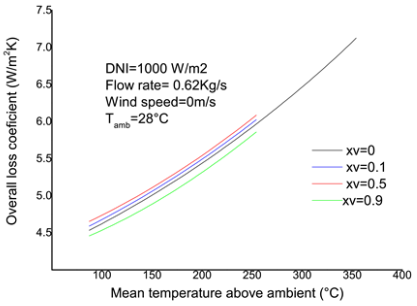

Fig. 16. Overall loss coefficient as a function of the amount of water vapor.

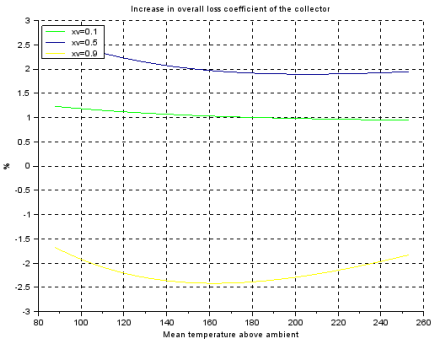

Fig. 17. Percentage variation of the overall loss coefficient.

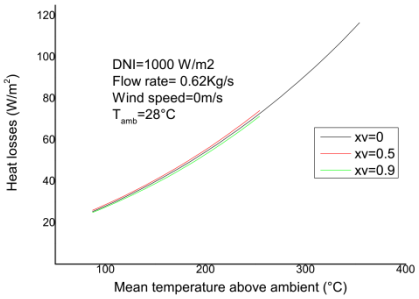

Fig. 18. Comparison of total heat losses between dry and humid environment

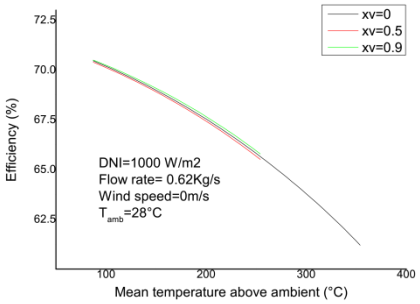

Fig. 19. Comparison of thermal efficiency between dry and humid environment

4. Conclusion

In this paper, we presented a numerical simulation of a parabolic trough collector based on a stationary physical model and general empirical correlations. The validity of the results is proven by comparison of the efficiency and thermal losses with experimental data obtained in Sandia laboratories in the USA. Therefore a detailed study about thermos-physical properties of humid air is carried out and integrated into the simulation program. We have found, on one hand that moisture doesn't affect transport properties of air at usual temperatures of the atmosphere. However, at high temperatures, they vary with the amount of water vapor with the exception of thermal expansion. These variations increase convective heat losses in the annulus in the case of low humidity and become closer to those of dry air for high humidity. On the other hand, we took into account the participation of water vapor on thermal radiation in the annulus. We have found that moisture decreases radiation heat losses in the annular space. Global thermal performances are slightly affected. In order to reach effective results, more experimental works are required to be performed.

Appendix A

Table A1. Coefficients for the calculation of the density of humid air [13,14].

$C_0 = 0.707$ $C_1 = -2.703 \times 10^{-2}$ $C_2 = 4.36 \times 10^{-3}$ $C_3 = -4.662 \times 10^{-5}$ $C_4 = 1.034 \times 10^{-6}$	$D_1 = 0.7 \times 10^{-8}$ $D_2 = -0.147 \times 10^{-8}$ $D_3 = -3.37568 \times 10^{-8}$
$E_1 = 0.104 \times 10^{-14}$ $E_2 = -0.335 \times 10^{-17}$ $E_3 = 3645.09$	$a = 1.007$ $b = -3.429 \times 10^{-3}$ $c = -3.439 \times 10^{-3}$

Table A2. Coefficients for the calculation of the viscosity of humid air [13,14].

$H_0 = 6.045$ $H_1 = 0.042$ $H_2 = -6.832$ $H_3 = 0.005$ $H_4 = -0.677$ $H_5 = -0.011$	$F_0 = -9.86 \times 10^{-1}$ $F_1 = 9.08 \times 10^{-2}$ $F_2 = -1.176 \times 10^{-4}$ $F_3 = 1.234 \times 10^{-7}$ $F_4 = -5.797 \times 10^{-11}$	$G_0 = 80.581$ $G_1 = 0.4$

Table A3. Coefficients for the calculation of thermal conductivity of humid air [13,14]

$I_0 = -2.276 \times 10^{-3}$ $I_1 = 1.259 \times 10^{-4}$ $I_2 = -1.481 \times 10^{-7}$ $I_3 = 1.735 \times 10^{-10}$ $I_4 = -1.066 \times 10^{-13}$ $I_5 = 2.476 \times 10^{-17}$	$M_0 = -0.568 \times 10^{-3}$ $M_1 = 0.108 \times 10^{-3}$ $M_2 = -7.395 \times 10^{-8}$ $M_3 = 3.73 \times 10^{-11}$
$L_0 = 31.997 \times 10^{-3}$ $L_1 = -0.133 \times 10^{-3}$ $L_2 = 3.816 \times 10^{-7}$ $L_3 = -2 \times 10^{-10}$	$J_0 = 17.617$ $J_1 = 5.558 \times 10^{-2}$ $J_2 = 5.558 \times 10^{-4}$

Table A4. Coefficients for the calculation of specific heat capacity of humid air [13,14]

$K_0 = 1.034$ $K_1 = -0.284 \times 10^{-3}$ $K_2 = 0.781 \times 10^{-6}$ $K_3 = -0.497 \times 10^{-9}$ $K_4 = 0.107 \times 10^{-12}$	$K_5 = 1.065$ $K_6 = -4.473 \times 10^{-4}$ $K_7 = 9.871 \times 10^{-7}$ $K_8 = 4.637 \times 10^{-10}$
$N_0 = 1.869$ $N_1 = -2.578 \times 10^{-4}$ $N_2 = 1.941 \times 10^{-5}$ $N_3 = 6.564$	$N_4 = -2.69 \times 10^{-2}$ $N_5 = 5.182 \times 10^{-5}$ $N_6 = -3.268 \times 10^{-8}$

Table A5. Parameters for equations (56)-(57) [15].

$a = -9.746 \times 10^{-1}$ $b_1 = 5.613 \times 10^{-5}$ $b_2 = 0$ $b_3 = 0$ $d_1 = 5.969 \times 10^{-1}$ $d_2 = -1.329 \times 10^{-1}$ $d_3 = 9.564 \times 10^{-3}$ $b_4 = -8.124 \times 10^{-4}$ $b_5 = 6.507 \times 10^{7}$ $b_6 = -2.574 \times 10^{-10}$ $d_4 = -8.523 \times 10^{-2}$ $d_5 = 0$ $d_6 = 0$	$a' = 1.549 \times 10^{-1}$ $b_1' = 1.753 \times 10^{-2}$ $b_2' = -8.847 \times 10^{-5}$ $b_3' = 0$ $d_1' = -1.634 \times 10^{-1}$ $d_2' = 2.544 \times 10^{-1}$ $d_3' = -7.691 \times 10^{-3}$ $b_4' = -4.628 \times 10^{-3}$ $b_5' = 2.674 \times 10^{-5}$ $b_6' = -1.48 \times 10^{-7}$ $d_4' = -1.491 \times 10^{-1}$ $d_5' = 2.292 \times 10^{-1}$ $d_6' = 0$

References

[1] M. G*ü*nther, M. Joemann, S. Csambor, A. Guizani, D. Kr*ü*ger, T. Hirsch, Parabolic trough collector, chapter 5 Advanced CSP teaching materials, 2011.

[2] MW. Edenburn, "Performance analysis of a cylindrical parabolic focusing collector and comparison with experimental results", Solar Energy, 18, pp. 437-444, April 1976.

[3] V. Dudley, G. Kolb, M. Sloan, D. Kearney, SEGS LS2 solar collector-test results, Report of Sandia National Laboratories, SANDIA94-1884, USA, 1994.

[4] R. Forristall, Heat transfer analysis and modelling of a parabolic trough solar receiver implemented in engineering equation solver, National Renewable energy Laboratory, 2003.

[5] Garcia-Valladares, N. Velázquez, "Numerical simulation of parabolic trough solar collector: Improvement using counter flow concentric circular heat exchangers", Int. J. Heat Mass Transfer, 52, pp. 597-609, 2009.

[6] Y. He, J. Xiao, Z. Cheng, Y. Tao, "A MCRT and FVM coupled simulation method for energy conversion processin parabolic trough solar collector, Renew. Energy, 36, pp. 976-985, 2011.

[7] A. Giostri, M. Binotti, M. Astolfi, P. Silva, E. Macchi, G. Manzolini, "Comparison of different solar plants based on parabolic trough technology", Solar Energy, 86, pp. 1208-1221, 2012.

[8] A. Abdollahpour, M. H. Ahmadi, A. H. Mohammadi, "Thermodynamic model to study a solar collector for its application to Stirling engines", Energy Conversion and Management, 79, pp. 666-673, 2014.

[9] M.Ouagued, A.Khellaf, L.Loukar, "Estimation of the temperature, heat gain and heat loss by solar parabolic trough collector under Algerian climate using different thermal oils", Energy Conversion and management, 91, pp. 321-336, 2013.

[10] F. Dittus, L. Boelter, "Publications on engineering", University of California, Berkeley, 26, 1930.

[11] V. Dudley, G. Kolb, M. Sloan, D. Kearney, SEGS LS2 solar collector-test results, Report of Sandia National Laboratories, SANDIA94-1884, USA, 1994.

[12] Dow chemical company, Syltherm 800, Heat transfer fluid, technical support data, September 2012. http://www.dow.com/heattrans/products/synthetic/syltherm.htm.

[13] P. Tsilingiris, "Thermophysical and transport properties of humid air at temperature range between 0 and 100 C", Energy Conversion and Management, 49, 1098-1110, 2008.

[14] C, A. Melling, S. Noppenberger, M. Still, H. Venzke, "Interpolation Correlations for Fluid Properties of Humid Air in the Temperature Range 100 C to 200 C", Journal of Physical and Chemical Reference Data, 26, 1111-1124, 1997.

[15] A. K. Mehrotra, K. Karan, L. A. Behie, "Estimate gas emissivities for equipment and process design", Chemical engineering progress, 91, pp. 70-77, 1995.

[16] W. W. Yuen, "Definition and Evaluation of Mean Beam Lengths for Applications in Multidimensional Radiative Heat Transfer: A Mathematically Self-Consistent Approach", Journal of Heat Transfer, 130, 2008.